Proceedings of the ASME 2010 3rd Joint US-European Fluids Engineering Summer Meeting and 8th International Conference on Nanochannels, Microchannels, and Minichannels
FEDSM-ICNMM2010
August 1-5, 2010, Montreal, Canada

FEDSM-ICNMM2010-30040

FLUID-STRUCTURE COUPLING IN GAS DAMPING RESPONSE OF NANOWIRE RESONATORS

Rustom B. Bhiladvala
University of Victoria
Victoria, BC, Canada
rustomb@uvic.ca

ABSTRACT

Nanowires vibrating at resonance in a gas can serve as sensitive detectors of mass ($< 10^{-18}$ grams), of use to molecular diagnosis of disease. They can also serve as sensitive detectors of damping force in an ambient gas environment. The Q-factor of resonance spectra, quantifies the sharpness of the peak and is a measure of the ratio of inertial to dissipative (damping) forces. Q-factor data enable quantification of the gas damping force in different regimes of rarefied gas dynamics. Measurements were made with silicon and rhodium nanowires of comparable size, in pure dry nitrogen, with pressure increasing from high vacuum (10^{-10} atm) to one atmospheric pressure. The data show that, for the silicon nanowires, the Q-factor begins to decrease from its high-vacuum value at a lower pressure and reaches a lower minimum value at one atmosphere, compared to the rhodium nanowires. We show that nanowire structural properties, namely the elastic modulus and intrinsic damping, are responsible for these differing sensitivities to a similar gas damping force range. The results show an important coupling of fluid and structural interaction for rarefied gas dynamics at nanoscale. For practical sensing applications in an ambient gas, this coupling indicates that silicon nanowires are better suited for gas damping force sensing, while rhodium nanowires would fare better as mass sensors for molecular diagnosis.

INTRODUCTION

Vibrating beams and wires at nanoscale have been proposed as the basis for instruments with unprecedented sensitivity. For example, nanowires (NWs) and nanotubes at resonance, owing to their small mass (~1 pg) and high resonant frequency (~1-100 MHz), yield measurable response to addition of mass below 10^{-18} g (1 atto-gram or ag) [1,2]. This indicates the possibility of their use for molecular diagnosis at an early stage of disease, when small concentrations of disease biomarker molecules are present. Accurate measurements of small mass with adequate signal-to-noise ratio require a sharp resonant peak, or a high quality factor (defined as in Eq 4 & Fig 2) for the resonance curve. The resonance Q-factor generally degrades significantly for motion in fluids, associated with high damping. This has motivated several attempts to offset air damping e.g. energy input through parametric laser pumping [3], using doubly-clamped beams in high tension [4] and using higher harmonics [5]. Several experimental studies [6-9] focus on improving our understanding of fluid damping of NWs.

From these reports, we observe that NWs from atmospheric pressure to a modest vacuum ~10^{-3} atm can serve as measuring instruments of gas damping force over a range of Knudsen number (gas molecule mean free path/wire diameter), $0.1<Kn<100$, spanning the transition and free molecular flow regimes of rarefied gas dynamics. Neither the continuum fluid approach nor simple models for molecular momentum transport can be trivially extended to work in the transition regime –the development of theoretical and computational models in this regime is currently a research area of significant interest [10-12]. Gas damping force measurements with nanowires can provide data for these models.

The challenge in measurements is that the high surface to volume ratio of nanostructures can cause an unusual and strong coupling of physical effects. Examples of such coupling involve transduction (vibration detection and driving) schemes, intrinsic stresses from fabrication and nonlinear geometric effects [13]. The recent introduction of a technique for nanoresonator directed-assembly [14], has enabled reduction of these modes of coupling. This allows focus on NW material property dependent effects in fluid structure interaction – specifically how NW density, elastic modulus and dissipation within the NW, affect measurements of gas damping and small mass.

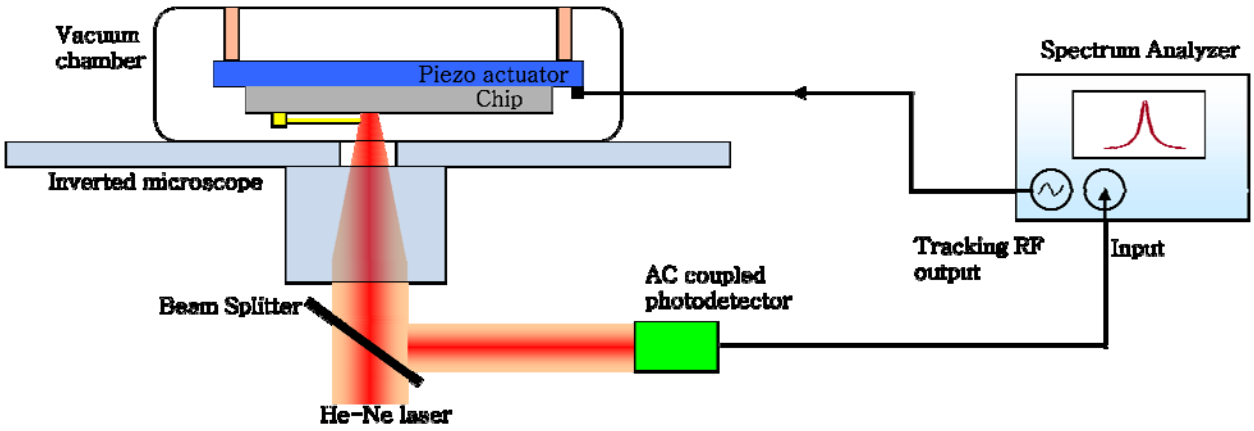

Figure 1: Schematic for nanowire resonance measurement. The chip with suspended nanowire resonators (representative nanowire shown in yellow) is mounted on a piezo actuator disc in a chamber with controls to vary pressure from 10^{-10} atm to 1 atm. The nanowire is forced into resonant vibration by a signal from the tracking generator of a spectrum analyzer. The signal could be applied to the piezo disc, or between nanowire and underlying pad, for electrostatic drive. A laser beam reflected off the chip as well as the vibrating nanowire generates an interference pattern that is converted to an electrical signal by a photo-detector and sent to the spectrum analyzer to produce the resonance spectrum.

NOMENCLATURE

f	Frequency
x	Displacement
ω	Angular frequency
C	Damping coefficient
F_0	Amplitude of forcing
K	Stiffness
M	Mass
X_s	Property X for structure
X_f	Property X for fluid
X_{s+f}	Property X for fluid+structure

EXPERIMENTAL METHODS

The nanowire resonance measurement setup uses a piezo drive and optical detection scheme as described in Figure 1. The driving signal is swept in a range about the peak frequency of a resonant mode. The peak frequency and the width are used for an experimental determination of the value of the Q-factor, as shown in Figure 2.

A single degree of freedom (SDOF) harmonically driven linear resonator model is adequate for understanding several key features of the fluid-structure interaction. The equation governing the displacement $\{x(t)\}$ of a resonator with mass M, damping C and stiffness K, driven harmonically at a forcing amplitude F_0 and frequency ω,

$$M\ddot{x} + C\dot{x} + Kx = F_0 \cos(\omega t) \qquad \textbf{(1)}$$

may be rewritten as

$$(M_s + M_f)\ddot{x} + (C_s + C_f)\dot{x} + (K_s + K_f)x = F_0 \cos(\omega t) \qquad \textbf{(2)}$$

with subscripts s and f referring to properties attributable to the solid NW and the ambient fluid, respectively. In the regimes of gas rarefaction we encounter, the added mass of ambient gas, M_f, carried by the resonator, is negligible [6]. In the absence of a spring stiffness component from a squeeze film, for cylindrical NW resonators, we may neglect K_f, to obtain

$$M_s\ddot{x} + (C_s + C_f)\dot{x} + K_s x = F_0 \cos(\omega t) \qquad \textbf{(3)}$$

The value of the Q-factor (Q) is evaluated experimentally as shown in Figure (2), and for Q>>1 may be related to the mass, resonance peak frequency and damping [Feynman], of Eq(1), by

$$Q = \frac{M\omega_n}{C} = \frac{\sqrt{MK}}{C}\ , \qquad \textbf{(4)}$$

where $\omega_n = 2\pi f_n$. The first measurement is made at high vacuum, with no gas damping (C_f =0), for which the Q-factor value, Q_s, depends only on the structural properties of the solid nanowire, M_s, C_s and K_s. Following this, the ambient gas pressure in the chamber was increased in steps, and the measurement repeated for each step. The resonance peak frequency shows negligible change, but the resonance curve width increases and the Q-factor, Q_{s+f} decreases, as the gas damping increase becomes significant. From Eq (4),

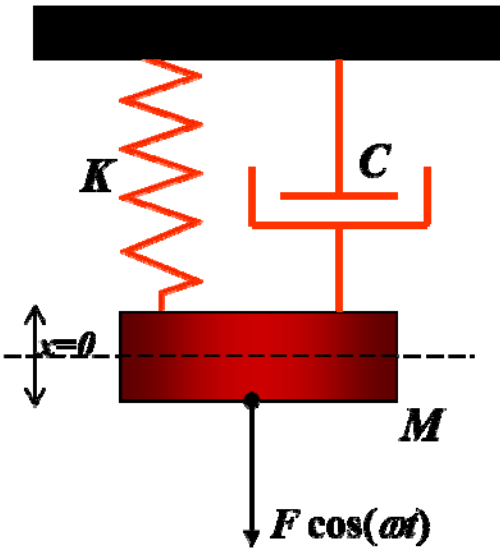

(a)

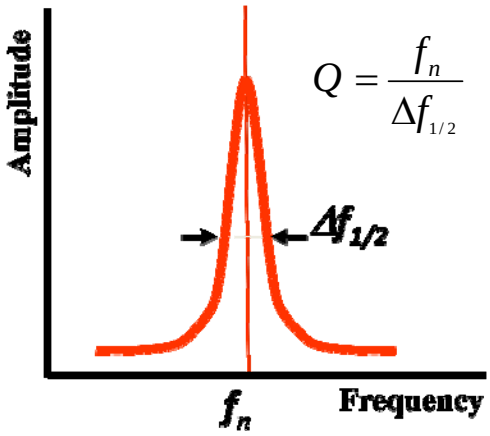

(b)

Figure 2 (a) Spring-mass-damper model for linear resonator described by Equation 1. **(b)** Resonance peak frequency f_n for mode n and the full width at half-maximum height of the power (amplitude^2) gives the experimental value for the quality factor, Q, if Q>>1.

$$Q_s = \frac{M_s \omega_n}{C_s} = \frac{\sqrt{M_s K_s}}{C_s},$$

$$Q_{s+f} = \frac{M_s \omega_n}{C_s + C_f} = \frac{\sqrt{M_s K_s}}{C_s + C_f}, \qquad \textbf{(5a \& b)}$$

from which, the Q-factor Q_{s+f} at any gas pressure is related to the high-vacuum value, Q_s, by

$$Q_{s+f} = Q_s \left(1 + \frac{C_f}{C_s}\right)^{-1}. \qquad \textbf{(6)}$$

The experiments were performed with two cantilevered nanowire resonators, one made of silicon (Si), and the other of metallic rhodium (Rh), which has a higher density and elastic modulus. The densities and measured geometric parameters, frequencies and high-vacuum Q-factors are listed in Table 1 below.

Table 1 Geometry, frequency, Q-factor for nanowires

Nanowire	Rh	Si
Dia d (μm)	0.28	0.33
Length L (μm)	5.8	11.8
Freq (MHz)	7.186	1.928
High vacuum Q_s	1080	4830
Density (kg/m^3)	12450	2330

Details of the hybrid nanofabrication scheme enabling metal nanowire cantilevers with consistent clamps to be fabricated, as well as spectra in vacuum and air may be found in Li et al.[14], and will not be repeated here. Nanoporous templates were used for the growth –electrodeposition was required for the rhodium nanowire and a different vapor-liquid-solid growth process for the silicon nanowire. Their lengths and diameters could not be closely matched. Tip fringe field electrostatic drive was used for the results presented. Q-factors were extracted using the best-fit Lorentzian curves (characteristic response of the linear, damped harmonic oscillator) to resonant spectra. The measurements for each data point were repeated at least three times, and during a single run, showed variations smaller than 1%. All resonant spectra were checked using reverse sweeps to ensure the absence of nonlinear stiffness effects.

In the results and analysis below, we focus on the role of geometry, density, elastic modulus and intrinsic dissipation within the nanowire material and their effects on performance of nanowires as rarefied gas sensors or mass sensors operating in air.

RESULTS

Figure 3 shows the Q-factor variation with ambient pressure for the NW cantilevers described in Table 1. As may be expected, each curve shows a decrease of Q-factor value as the damping increases with pressure. The RhNW cantilever has a vacuum Q-factor of the same order of magnitude as the SiNW. As the ambient pressure is increased, the initiation point of the reduction in vacuum value of the Q-factor occurs at a higher pressure for the RhNW and the reduction is more gradual than for the SiNW, with Q at 1 atm being about 1/5th of the high vacuum value, compared to 1/250th for the SiNW . We center

our discussion of fluid-structure interaction on Q-factor values at three points on each curve, as shown in Figure 3. $Q_{Si,s}$ and $Q_{Rh,s}$ are the same as the high vacuum values listed in Table 1, in regions where fluid damping is not significant. $Q_{Si,i}$ and $Q_{Rh,i}$ are Q-factor values at pressures marking the initiation of a rapid decrease in Q-factor with increasing pressure. These are technologically important as they identify the vacuum level for nanostructure vibration to be unaffected by air damping –and dictate the sophistication and cost of pumping equipment required for nanostructures to see negligible effects of gas damping. What determines the pressure locations for these points?

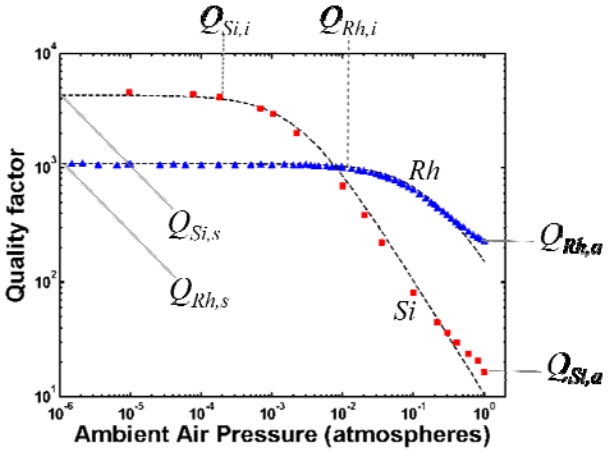

Figure 3 Measured Quality factor variation with ambient pressure for silicon and rhodium nanowires.

The SiNW is about the same diameter but twice as long as the RhNW. Could this fact alone lead to a high enough air damping to account for the SiNW's lower pressure initiation of Q-factor decline? Could it also account for the steeper decline for the SiNW at higher pressures, with Q-values at 1 atm pressure $Q_{Si,a} << Q_{Rh,a}$? How best could we use the observed difference between Si and RhNWs to advantage for sensing applications? Some answers to these questions will emerge from a consideration of the structural and fluid damping behavior of the Rh and SiNWs, presented in the following discussion.

DISCUSSION

It will be useful to begin by examining some calculated geometric/structural parameters in Table 2 below.

Using results for rarefied gas dynamics reported earlier [6], we note that below 0.2 atm pressure, the Knudsen number (=gas mean free path/wire dia), Kn > 10, so that the free molecular flow expression [6] for fluid damping coefficient $C_f = 2\rho_f U_{th} L d$ applies. Here U_{th} is the gas molecule velocity, dependent on temperature, and fluid density ρ_f ~ pressure. If fluid damping difference due to NW lengths alone were responsible for the pressures at which the Q-degradation begins, then this pressure for the SiNW, which is twice as long, should be about half that for the RhNW –however the factor is about a hundredth, as seen in Figure 3, so this conjecture cannot be supported.

Table 2 NW Geometric and Structural Parameters

Nanowire	Rh	Si
Surface Area, A (m^2)	5.10×10^{-12}	1.22×10^{-11}
Volume, V (m^3)	0.357×10^{-18}	1.01×10^{-18}
Surf. Area / Vol ratio, A_s/V (m^{-1})	1.43×10^{7}	1.21×10^{7}
Solid Mass, M_s (kg)	4.45×10^{-15}	2.35×10^{-15}
Angular Freq, ω (rad/s)	4.52×10^{7}	1.21×10^{7}
$M_s\omega$ (kg/s)	2.01×10^{-7}	2.85×10^{-8}
Str. Damping, $C_s = M_s\omega/Q_s$ (kg/s)	1.86×10^{-10}	5.90×10^{-12}

If fluid damping difference due to NW lengths alone were responsible for the pressures at which the Q-degradation begins, then this pressure for the SiNW, which is twice as long, should be about half that for the RhNW –however the factor is about a hundredth, as seen in Figure 3, so this conjecture cannot be supported.

Theoretical understanding of what determines structural damping C_s, within the NW material, is an active area of current research [15,16]. We note the value for the RhNW is ~32 times that for the SiNW –however the ratios for the first four parameters in the table are between 1 and 2, so that the ratio of C_s values is far from being in simple proportion to the ratios of masses or of these geometric parameters. It is qualitatively reasonable to assert that, compared to nearly single-crystal Si, the large grain boundary volume fraction in a fine-grained, high melting point metal such as Rh may result in a much higher damping coefficient. The damping coefficient of Rh should lead to a vacuum Q-value which is ~ 0.03 that of Si, but the higher density (ρ_s) and elastic modulus (E) of Rh offset this considerably $\{M_s\omega \sim (E\rho_s)^{0.5}\}$ [6], so that $Q_{s,Rh}$ ~ 0.22 $Q_{s,Si}$, from Equation 5(a).

The high intrinsic damping of the RhNW plays a strong role in determining the initiation pressure for Q-factor decrease seen in Figure 3, as well as in the rate of change of Q at higher pressures. For initiation, we may consider Eq (6) and ask when Q_s/Q_{s+f} ~ 0.99? This occurs when fluid damping C_f/C_s ~ 0.01 . Using the length, diameter and C_s value for the Rh and SiNWs and the free molecular flow expression for fluid damping C_f, we obtain an initiation pressure for Rh ~ 75 times that for Si, closer to the observed data in Figure 3. Equation 6 also shows the rate of change of Q_s/Q_{s+f} varies with the ratio C_f/C_s –a given increase in fluid damping will cause a smaller degradation in Q-factor, if the intrinsic damping C_s has a higher value. This is confirmed by the gentler roll-off seen for the RhNW in Figure 3.

CONCLUDING REMARKS

High structural damping C_s may thus have a positive role to play in some types of sensors. For small mass sensing, applicable to areas such as molecular diagnosis, both the signal to noise ratio of the resonance measurement ($\sim Q^{0.5}$) as well as the accuracy of resonance peak frequency location required for mass measurement at near-atmospheric pressure are improved by maintaining a high Q value. Devices with high intrinsic damping *as well as* high density-modulus product values, such as RhNWs, would be better suited to that purpose. The SiNW has a higher spread in Q-values (max/min ~ 250) and shows the same relative response to far smaller (~1/32 times that of RhNW, in this example) changes in fluid damping, and will thus be a more sensitive instrument for measuring gas damping force in the transition regime, to improve understanding of rarefied gas dynamics.

We note that we have here not considered resonance in environments such as dense gases or liquids [8], where the damped resonance frequency may change appreciably due to much larger damping C_f, leading to a two-way fluid-structure interaction. In conclusion, interaction between fluid damping and structural properties arising from geometry and nature of the material are important in the design and choice of application of nanoresonant sensors operating in a fluid environment.

ACKNOWLEDGEMENTS

Financial support for this work from the US National Institutes of Health and the NSERC (Canada) is gratefully acknowledged. The analysis in this work is based on experimental data[14]. The support of the authors listed in Ref [14] in obtaining these data is gratefully acknowledged.

REFERENCES

[1] Naik, A. K., Hanay, M. S., Hiebert W.K., Feng X.L. and Roukes M.L., 2009, "Towards Single-Molecule Nanomechanical Mass Spectrometry," Nature Nanotechnology, 4, pp 445-449.

[2] Peng, H. B., Chang, C. W., Aloni, S., Yuzvinsky, T. D. and Zettl, A., 2006, "Ultrahigh frequency nanotube resonators," Phys. Rev. Lett. 97, Article Number: 087203.

[3] Sekaric, L., Zalalutdinov, M., Bhiladvala, R. B., Zehnder, A. T., Parpia, J. M. and Craighead, H.G., 2002, "Operation of Nanomechanical Resonant Structures in Air," Appl. Phys. Lett, 81(14), pp. 2641-2643.

[4] Verbridge, S. S., Craighead, H. G., Parpia, J. M., 2008, "A Megahertz Nanomechanical Resonator with Room Temperature Quality Factor Over a Million," Appl. Phys. Lett., 92(1), Article Number: 013112.

[5] Naik, T., Longmire, E. K. and Mantell, S. C., 2003, "Dynamic response of a cantilever in liquid near a solid wall," Sensors and Actuators A, 102(3), pp. 240-254.

[6] Bhiladvala, R. B., and Wang, Z. J., 2004, "Effect of Fluids on the Q Factor and Resonance Frequency of Oscillating Micrometer and Nanometer Scale Beams," Phys. Rev. E, 69, Article Number: 036307

[7] Karabacak, D. M., Yakhot, V. and Ekinci, K. L., 2007, "High-frequency nanofluidics: An experimental study using nanomechanical resonators," 98(25), Article Number: 254505

[8] Svitelskiy, O., Sauer, V., Liu, N., Cheng, K. M., Finley, E., Freeman, M. R., Hiebert, W. K., 2009, "Pressurized Fluid Damping of Nanoelectromechanical Systems," Phys. Rev. Lett., 103(24), Article Number: 244501

[9] Li, M., Tang, H. X. and Roukes, M. L., 2007, "Ultra-sensitive NEMS-based Cantilevers for Sensing, Scanned Probe and Very High-Frequency Applications," Nature Nanotechnology, 2**,** pp. 114-120 .

[10] Ramanathan, S. and Koch, D.L., 2009, "An Efficient Direct Simulation Monte Carlo Method for Low Mach Number Noncontinuum Gas Flows Based on the Bhatnagar-Gross-Krook Model ," Phys. Fluids, 21(3), Article Number: 033103

[11] Torrilhon, M. and Struchtrup, H., 2004, "Regularized 13-moment Equations: Shock Structure Calculations and Comparison to Burnett Models," J. Fluid Mech., 513, pp 171-198.

[12] Zheng, Y. S., Reese, J. M., Struchtrup, H., 2006, "Comparing Macroscopic Continuum Models for Rarefied Gas Dynamics: A New Test Method," J. Comput. Phys., 218(2), pp. 748-769

[13] Sahai, T., Bhiladvala, R. B. and A.T. Zehnder, 2007, "Thermomechanical Transitions in Doubly-Clamped Micro-oscillators," Int. J. Nonlinear Mech., 42, pp. 596-607.

[14] Li, M. W., Bhiladvala, R. B., Morrow, T.J. et al., 2008, "Bottom-up Assembly of Large-area Nanowire Resonator Arrays," Nature Nanotechnology, 3(2), pp. 88-92.

[15] Kim, S. Y., Park, H. S., 2008, "Utilizing Mechanical Strain to Mitigate the Intrinsic Loss Mechanisms in Oscillating Metal Nanowires," Phys. Rev. Lett., 101(21), Article Number: 215502.

[16] Ru, C.Q., 2009, "Size Effect of Dissipative Surface Stress on Quality Factor of Microbeams," Appl. Phys. Lett., 94(5), Article Number: 051